

Response of a Coupled Ocean–Atmosphere Model to Increasing Atmospheric Carbon Dioxide: Sensitivity to the Rate of Increase

RONALD J. STOUFFER

NOAA/Geophysical Fluid Dynamics Laboratory, Princeton, New Jersey

SYUKURO MANABE

Institute for Global Change Research, Frontier Research System for Earth Sciences, Tokyo, Japan

(Manuscript received 2 February 1998, in final form 20 July 1998)

ABSTRACT

The influence of differing rates of increase of the atmospheric CO₂ concentration on the climatic response is investigated using a coupled ocean–atmosphere model. Five transient integrations are performed each using a different constant exponential rate of CO₂ increase ranging from 4% yr⁻¹ to 0.25% yr⁻¹. By the time of CO₂ doubling, the surface air temperature response in all the transient integrations is locally more than 50% and globally more than 35% of the equilibrium response. The land–sea contrast in the warming, which is evident in the equilibrium results, is larger in all the transient experiments. The land–sea difference in the response increases with the rate of increase in atmospheric CO₂ concentration. The thermohaline circulation (THC) weakens in response to increasing atmospheric CO₂ concentration in all the transient integrations, confirming earlier work. The results also indicate that the slower the rate of increase, the larger the weakening of the THC by the time of doubling. Two of the transient experiments are continued beyond the time of CO₂ doubling with the CO₂ concentration maintained at that level. The amount of weakening of the THC after the CO₂ stops increasing is smaller in the experiment with the slower rate of CO₂ increase, indicating that the coupled system has more time to adjust to the forcing when the rate of CO₂ increase is slower. After a period of slow overturning, the THC gradually recovers and eventually regains the intensity found in the control integration, so that the equilibrium THC is very similar in the control and doubled CO₂ integrations. Considering only the sea level changes due to the thermal expansion of seawater, the integration with the slowest rate of increase in CO₂ concentration (i.e., 0.25% yr⁻¹) has the largest globally averaged sea level rise by the time of CO₂ doubling (about 42 cm). However, only a relatively small fraction of the equilibrium sea level rise of 1.9 m is realized by the time of doubling in all the transient integrations. This implies that sea level continues to rise long after the CO₂ concentration stops increasing, as the warm anomaly penetrates deeper into the ocean.

1. Introduction

Due to uncertainty in the world's rate of economic development, the future rates of increase in the atmospheric concentrations of greenhouse gases are highly uncertain. It is therefore important to study how the climatic response depends upon the growth rates of the various greenhouse gases. One can speculate that the climatic response to a very rapid increase in climatic forcing may be very different from the response to a very slow increase due to differences in the depth to which anomalies penetrate in the ocean. Differences in the penetration depth result in changes in the effective heat capacity of the ocean (e.g., Manabe et al. 1991,

hereafter referred to as M91). The necessity to investigate the dependence of the coupled system response upon the growth rate in the climate forcing also arises because of the possibility of large climate changes associated with a marked change in the intensity of the thermohaline circulation (M91; Manabe and Stouffer 1994, hereafter referred to as M94).

The climatic response to increased greenhouse gas concentrations in the atmosphere has been under investigation for more than 30 yr. Over the past 10 yr or so, a number of studies have been conducted on the time-dependent (so-called transient) response of the coupled ocean–atmosphere system to the increase in the concentration of carbon dioxide (e.g., Stouffer et al. 1989; Washington and Meehl 1989; M91; Cubasch et al. 1992; Murphy and Mitchell 1995). All these studies use an equivalent amount of CO₂, which has the same radiative forcing as all the greenhouse gases combined. Washington and Meehl assume a constant linear rate of CO₂ increase of 1% yr⁻¹. The other three studies use a constant ex-

Corresponding author address: Mr. Ronald J. Stouffer, NOAA/Geophysical Fluid Dynamics Laboratory, Forrester Campus, U.S. Route 1, P.O. Box 308, Princeton, NJ 08542.
E-mail: rjs@gfdl.gov

ponential rate of CO₂ increase, which corresponds approximately to a constant rate of increase in the climatic forcing. The studies of Manabe et al. and Mitchell et al. use a rate of CO₂ increase of 1% yr⁻¹ compounded, while Cubasch et al. used the IPCC 1990 scenario A, which is similar to the 1% yr⁻¹ increase, compounded. Recently a number of coupled model studies (e.g., Mitchell et al. 1995; Meehl et al. 1996; Haywood et al. 1997) have incorporated estimates of past and future radiative forcings. The rate of increase in the radiative forcing in these scenarios is highly variable in time.

The purpose of this paper is to investigate in a systematic way how the response of the fully coupled, three-dimensional ocean-atmosphere model depends upon the rate of increase in the atmospheric concentration of CO₂. For simplicity, only changes in the atmospheric CO₂ concentration are used to force the model response. Five different transient integrations are performed, each using a different rate of increase in the atmospheric CO₂ concentration. Throughout each individual integration the exponential rate of increase in the atmospheric CO₂ concentration is held constant, producing an approximately constant rate of increase in the radiative forcing. Our analysis of the time-dependent climate change is mainly focused on comparing the climate response at the time of CO₂ doubling in the atmosphere, when the radiative forcing becomes the same in all the transient integrations. This allows for a quantitative comparison of the climate change realized in each integration.

To study the evolution of the climate response after the time of doubling, two of the transient integrations are extended holding the atmospheric CO₂ concentration constant at twice its normal value. Furthermore, one of these integrations is continued until the climate system stops changing systematically and is in equilibrium with the radiative forcing. This equilibrium integration yields important insights when compared to the transient integrations. By the time of doubling, the transient experiment using the slowest rate of CO₂ increase should have the largest response, because the coupled system has more time to approach the equilibrium state. An important part of this paper is to estimate quantitatively the fraction of the transient response to the equilibrium response.

The model structure is discussed in the subsequent section, followed by a description of the experimental design including the initialization procedure used to start the coupled model. The transient response of the coupled atmosphere-ocean system is then compared to the equilibrium response. Conclusions are drawn in the last section.

2. Model structure

Only a brief description of the model structure is given here. For a more detailed description see M91. The coupled model consists of general circulation mod-

els (GCM) of the atmosphere and oceans, and a land surface model. It is a global model with realistic geography limited by its grid resolution. It has nine vertical finite-difference levels. The horizontal distributions of predicted variables are represented by spherical harmonics (15 associated Legendre functions for each of 15 Fourier components) and by gridpoint values (Gordon and Stern 1982). A simple land surface model is used to compute surface fluxes of heat and water (Manabe 1969). Insolation varies seasonally, but not diurnally. The model predicts cloud cover, which depends only on relative humidity.

The ocean GCM (Bryan and Lewis 1979) uses a full finite-difference technique and has a regular grid system with approximately a 4° lat × 3.7° long spacing. There are 12 vertical finite-difference levels. The atmospheric and oceanic components of the model interact with each other once each day through the exchange of heat, water, and momentum fluxes. A simple sea ice model is also incorporated into the coupled model. It predicts only sea ice thickness computed from a thermodynamic heat balance and the advection of ice by ocean currents. For further details about the coupled model and a comparison of the model simulation with observations (M91). Dixon et al. (1996) also describe the ability of the model to simulate the uptake of anthropogenic trichlorofluoromethane (CFC-11) by the ocean.

This coupled model has been used to study the effects of increasing greenhouse gases on the climate (Stouffer et al. 1989; M91; Manabe et al. 1992; M94), natural variability of the coupled system (Delworth et al. 1993, 1997; Manabe and Stouffer 1996; Knutson et al. 1997), and abrupt climate change (Manabe and Stouffer 1995, 1997).

3. Numerical integrations

a. Transient integrations

Starting from an initial condition in a quasi-equilibrium state, the standard or control time integration of the coupled model is performed with a constant concentration of atmospheric carbon dioxide. This quasi-equilibrium condition is obtained by separate time integrations of the atmospheric and oceanic components of the model using observed surface boundary conditions (sea surface temperature, sea surface salinity, and sea ice thickness). The convergence of the oceanic component toward equilibrium is accelerated by the method described in Bryan (1984). These acceleration methods are not used when the atmospheric and oceanic model components are coupled. The coupled model integration is then continued for more than 1000 model yr.

When the time integration of a coupled model starts from the initial conditions identified above, the model climate drifts toward its own less realistic equilibrium state. To reduce the drift, the fluxes of heat and water at the ocean-atmosphere interface are adjusted by given amounts before they are imposed upon the oceanic sur-

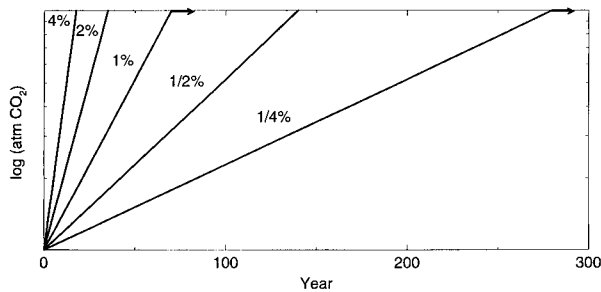


FIG. 1. Schematic of the logarithm of atmospheric CO₂ concentration vs time (yr) for the various integrations.

face (M91). These adjustments do not change from one year to the next and are independent of the anomalies of temperature and salinity at the oceanic surface, which develop during the integration of the coupled model. Thus they neither systematically damp nor amplify any surface anomalies, which occur during the integration. Although the adjustments do not eliminate the shortcomings of model dynamics or thermodynamics (Marotzke and Stone 1995), they do help prevent the rapid drift of the model from the initial state. Such drift can seriously distort sensitivity experiments such as those described below.

The results of Gregory and Mitchell (1997) highlight this fact. They ran two coupled model experiments with and without flux adjustments. They found that the magnitude of surface air temperature response to increasing CO₂ in the atmosphere was distorted in the model, which did not use flux adjustments. Fanning and Weaver (1997) also found that the geographical pattern of the surface air temperature response to increasing CO₂ is different, with and without the use of flux adjustments. We suspect that the difference may be attributable to the distorted control climate, which has unrealistic coverages of sea ice and snow cover as noted by Gregory and Mitchell. Obviously, it is highly desirable to develop a coupled model that can maintain a realistic control climate in the absence of flux adjustments. However in trying to obtain a realistic climate, one has to guard against the temptation to overturn one component of the model in order to make up for shortcomings in other model components.

The initial conditions for the control integration have realistic seasonal and geographical distributions of surface temperature, surface salinity, and sea ice thickness, with which both the atmospheric and oceanic components of the model are nearly in equilibrium (M91). The initial conditions used for the transient response integrations are the states of the coupled model at various times near the beginning of the 1000-yr control integration. For all the results described here, identical flux adjustments are applied to all integrations.

There are five transient integrations (Fig. 1) with differing rates of increase of the atmospheric CO₂ concentration: 4%, 2%, 1%, 0.5%, and 0.25% yr⁻¹. The

TABLE 1. The averaging periods used for the various integrations.

Integration	Years averaged	Control averaging period
4%	16–20	Years 1–100 of the control
2%	31–40	Years 1–100 of the control
1%	61–80	Years 1–100 of the control
0.5%	131–150	Years 101–200 of the control
0.25%	271–290	Years 201–300 of the control
2X	3901–4000	Years 3901–4000 of the control

integration in which the rate of increase of the atmospheric CO₂ concentration is 0.25% yr⁻¹ compounded will be called the 0.25% integration. A similar naming convention holds for the other transient integrations. As shown schematically in Fig. 1, the time required for a doubling of the atmospheric CO₂ concentration is 17.5 yr, 35 yr, 70 yr, 140 yr, and 280 yr for the 4%, 2%, 1%, 0.5%, and 0.25% integrations, respectively. Since the radiative forcing of the increasing CO₂ concentration is approximately proportional to the logarithm of the CO₂ concentration, the increase in the radiative forcing in these experiments is almost linear with respect to time. The 1% and 0.25% integrations are extended for several centuries holding the CO₂ concentration fixed at twice its normal value in order to study the climatic response of the coupled system beyond the time of doubling. The 1% integration is the same as the 2XC integration of M94.

For the analysis of the various integrations (Table 1), it is important that the time periods used in the averaging be as long as possible. For the 1%, 0.5%, and 0.25% integrations, a 20-yr time average centered on the time of CO₂ doubling is used. The time averaging period for the 2% and 4% integrations are 10 and 5 yr, respectively. (For this computation, all the transient integrations are extended for a 10-yr period beyond the doubling time, holding the CO₂ concentration constant at twice its normal value.) These relatively long averaging periods reduce the effect of natural variability in the time-mean quantities and thereby in the differences (perturbed minus control). In addition to presenting time averages at the time of doubling, the time series of annually averaged values of a given variable are shown from the beginning of the integration to the time of CO₂ doubling, allowing the comparison of the response at any given time. Because the control and equilibrium 2X-integrations have very little drift in the surface air temperature when they reach equilibrium, century time averages are used when presenting results from these integrations. The use of century time averages further reduces the effects of natural variability on the results shown here.

b. Equilibrium integration

To obtain the doubled CO₂ equilibrium climate and compare it to the transient response to CO₂ doubling, the 2XC integration of M94 is continued. In this inte-

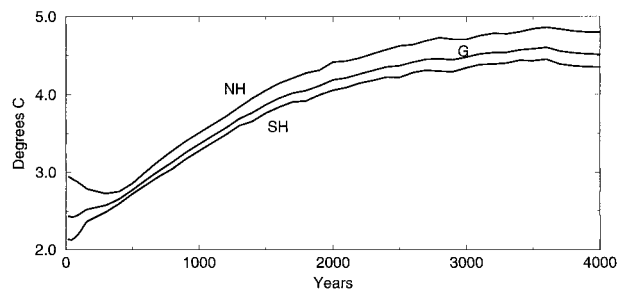


FIG. 2. 4000-yr time series of the Northern Hemisphere (top line), global (middle line), and Southern Hemisphere (bottom line) mean temperature ($^{\circ}\text{C}$) at a depth of 2935 m obtained from the oceanic component of the coupled model for the equilibrium 2X-integration.

gration, the CO_2 concentration increases at a compounded rate of $1\% \text{ yr}^{-1}$ until the concentration is twice the normal amount. Then the model is integrated for a total of 4000 yr with the CO_2 concentration kept constant. In this paper, this integration will be called the equilibrium 2X-integration. Near the end of the 4000-yr integration, the globally and hemispherically averaged ocean temperatures at a depth of approximately 3 km are hardly changing (Fig. 2). Since the deepest layers of the ocean have the longest response times to changes in the surface forcing, the model is very near a steady-state climate. This demonstrates that the model is nearly in equilibrium with the increased atmospheric CO_2 concentration.

Figure 2 also indicates that temperature decreases slightly near the beginning of the time series, especially in the Northern Hemisphere. During this part of the experiment, the thermohaline circulation (THC) in the Atlantic Ocean weakens temporarily (M94). In the deepest levels of the Atlantic, relatively cold Antarctic water replaces the North Atlantic Deep Water, producing the cooling of the hemispheric mean. However, by the end of the experiment one can see that the coupled model climate is nearly in equilibrium as noted above.

4. Equilibrium response

To assess the response of the transient integrations with varying rates of CO_2 increase, a brief description of the results obtained from the 2X-integration are shown. The equilibrium response of the coupled model will be investigated further in forthcoming papers. The globally averaged surface air temperature change due to CO_2 doubling in the coupled model is 4.5 K, while this value is 3.7 K for a comparable atmosphere-mixed layer ocean model in which the oceanic heat transport is prescribed implicitly and does not change in response to the doubled CO_2 in the atmosphere (M91). The larger response in the coupled model seems to occur mainly because of its larger climate sensitivity. The larger climate sensitivity results from a cooling trend in the globally averaged surface air temperature, which occurs during the first 2000 yr of the coupled integration, after

that time there is little or no drift. The trend results in the globally averaged surface air temperature being about 0.7 K cooler near the end of the control integration of the coupled model than in the control integration of the atmosphere-mixed layer ocean model. The cooler climate in the coupled model results in more extensive sea ice coverage and thicker sea ice, leading to a larger snow-ice-albedo feedback and a larger climate sensitivity to increased CO_2 (Spelman and Manabe 1984). Were the state attained toward the end of the control integration of the coupled model warmer and more realistic, the equilibrium response of the global mean surface air temperature to the doubling of atmospheric CO_2 (i.e., 4.5 K) would be closer to the corresponding response in the atmosphere-mixed layer ocean model (i.e., 3.7 K). Therefore, we are uncertain whether the equilibrium response of the coupled model with a more realistic control climate is significantly larger than that of the atmosphere-mixed layer ocean model. One should also note that the coupled model does not include some of the important processes that could affect the sensitivity of climate such as the changes in continental ice sheets and vegetation. The reliable, quantitative determination of the equilibrium response of the actual climate system remains a subject of future investigation.

The equilibrium surface air temperature response to the doubled CO_2 concentration in the atmosphere (Fig. 3) is similar in pattern over most regions to previous atmosphere-mixed layer ocean models (Mitchell et al. 1990). The warming in the low latitudes is smaller than in high latitudes, the so-called polar amplification of the surface temperature response. An exception is found in the region just southwest of Australia where the warming is at a minimum. Apparently, changes in the vertical mixing cause this minimum in the surface air temperature. Analysis of the surface temperature time series from the 2X-integration indicates that surface air temperatures in this region were unchanged over the last few hundred years of the integration, indicating that it is likely that the coupled system is in equilibrium with the forcing.

A land-sea contrast in the warming is also evident (Fig. 3), with the warming generally larger over the continents than over the oceans at the same latitude. This land-sea contrast was also found in the response obtained from atmosphere-mixed layer ocean models (Mitchell et al. 1990). As described by Manabe et al. (1992), this contrast is mainly due to two causes. First, the continental surfaces are drier than oceanic surfaces. Thus a larger fraction of the increase in radiative energy received by the earth's surface results in a relatively larger increase in sensible rather than latent heat, yielding a larger increase of surface air temperature over the continents. Furthermore, the continents tend to become drier during the summer mainly in response to the increased evaporation resulting from the increased radiative energy at the earth's surface, leading to an even

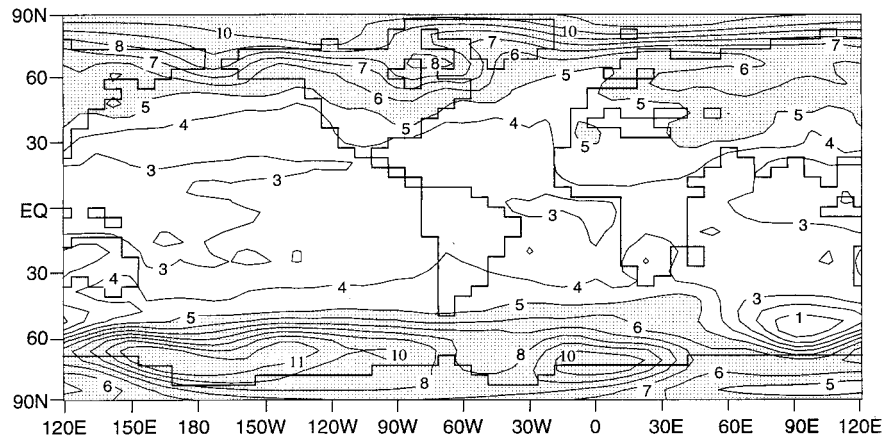


FIG. 3. Geographical distribution of the surface air temperature difference (K) between the 2X-equilibrium and control integrations for the years 3901–4000. The contour interval is 1 K.

larger increase in surface air temperature (Manabe et al. 1981).

Second, the coverage of snow over the continents is much more extensive than that of sea ice over the oceans during the colder half of the year in the control integration. Thus as the climate warms, the snow albedo feedback process over the continents is more effective than over the sea ice albedo feedback process in middle latitudes. In the Northern Hemisphere poleward of about 40°N, the land–sea contrast seen in the annually averaged response (Fig. 3) is mainly attributable to the snow albedo feedback process during winter and spring. To the south of this latitude, it is mostly attributable to smaller evaporative cooling of the continental surface discussed above.

As will be shown later, the high-latitude, equilibrium response of surface air temperature of the coupled model

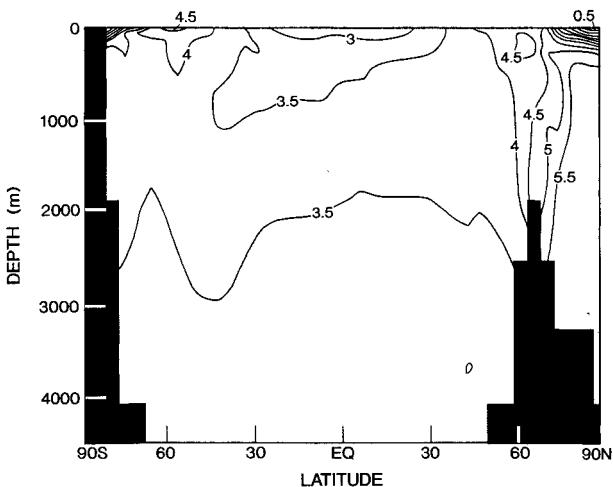


FIG. 4. Latitude depth distribution in the difference of zonal-mean temperature (K) between the equilibrium and control integrations for the years 3901–4000. The contour interval is 0.5 K. Negative values are shaded.

is much larger and quite different from its transient response to the increase of CO₂ concentration in the atmosphere (Gates et al. 1992). In the transient integrations, the effective thermal inertia is very large and surface warming is very small in the extreme North Atlantic and the Circumpolar Ocean of the Southern Hemisphere, because of the downward penetration of the warm anomalies into the oceans (M91). On the other hand, these regions of small warming are not evident in the equilibrium integration, because sufficient time is available for the whole volume of the ocean to equilibrate with the radiative forcing.

By the time the 2X-integration reaches equilibrium, the warming is large and remarkably uniform throughout the volume of the ocean (Fig. 4). Near the ocean surface, the warming is at a maximum near 50°S and 65°N. In regions of sea ice in both polar regions, there is a minimum in the warming near the surface due to the presence of sea ice, which anchors the temperature near the freezing point of seawater in the control and 2X-integrations. This minimum is very shallow due to the halocline, which exists under the sea ice. The weak maximum in the warming seen around the depth of 1.5 km over most latitudes in this zonally averaged section is found mainly in the Atlantic Ocean. This is apparently the result of changes in the depth of the outflow of the THC. In spite of these few regions where the temperature response is different from 3.5 K, the uniformity of the warming throughout the entire depth of the World Ocean is remarkable.

5. Transient response

a. Surface air temperature

The rate of increase in the annually averaged global mean surface air temperature (SAT) is directly related to the rate of increase in the atmospheric CO₂ concentration (Fig. 5). The 4% integration has the fastest rate

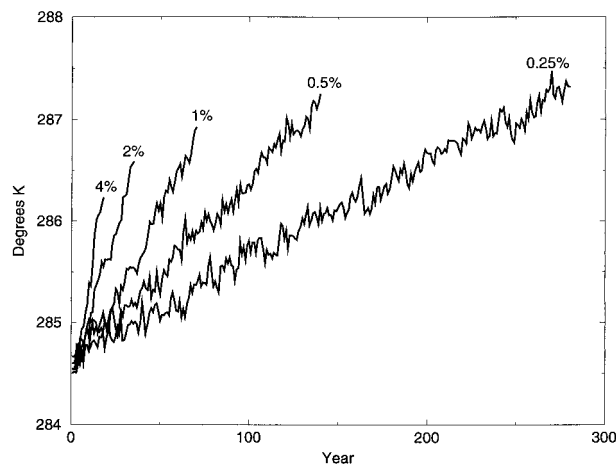


FIG. 5. Time series of global mean surface air temperature (K) for the various integrations. Time is given in years.

of increase of SAT, and the 0.25% integration has the slowest rate of increase. However, by the time of CO_2 doubling, one sees that a larger fraction of the warming is realized with the slower rate of increase in the CO_2 concentration (see Table 2 and Fig. 5). The integration with slowest rate of increase of CO_2 , the 0.25% integration, produced the largest globally averaged change in SAT, 2.6 K. This is about 58% of the warming realized when the coupled model is run to equilibrium with doubled CO_2 concentration in the model's atmosphere. The fastest rate of increase of atmospheric CO_2 produced the smallest temperature increase at doubled CO_2 , 1.5 K. These results indicate that at the time of doubling, the slower the rate of increase in atmospheric CO_2 concentration, the closer the response of SAT is to the equilibrium value, as expected.

As will be shown later, the temperature anomaly due to increasing CO_2 penetrates deeper into the world's ocean for the integrations with the slower rates of CO_2 increase and, therefore, more heat is sequestered in the ocean. However, the slower rate of increase of atmospheric CO_2 also allows more time for the upper ocean to adjust toward the full equilibrium response than in the integrations using the more rapidly increasing CO_2 concentrations. So the response of the surface temperature achieved before the doubling of atmospheric CO_2 is larger, even though a larger fraction of the heat is sequestered in the deep ocean.

The large-scale patterns of surface air temperature response (Fig. 6) are similar between the various integrations. The warming is relatively large over the middle and high latitude continents and relatively small over the Tropics and the midlatitude oceans. In the integrations with slower rates of CO_2 increase, the warming is a maximum over the Arctic Ocean. The warming is at a minimum in the northern North Atlantic and Circumpolar Oceans of the Southern Hemisphere in all the transient integrations as shown earlier (M91). These ar-

TABLE 2. Global surface air temperature response of the various integrations at the time of doubled CO_2 concentration in the atmosphere. DSAT is the annually averaged surface air temperature difference (K) between the given integration and the control at doubling time. The averaging period of each experiment is shown in Table 1. Equil. Cpld integration is the equilibrium 2X-integration. FRAC is the fraction of the equilibrium coupled model surface air temperature response to a doubling of CO_2 .

Avg. Period (years)	131–					Equil. Cpld
	271–290	150	61–80	31–40	16–20	
Exp. Name	0.25%	0.5%	1%	2%	4%	Equil. Cpld
DSAT	2.6	2.4	2.2	1.8	1.5	4.5
FRAC	0.58	0.53	0.49	0.40	0.33	1.0

eas are regions of deep vertical mixing of heat into the ocean, which greatly increases the effective heat capacity in these regions. Over most areas north of 30°S , about 70% of the total equilibrium response is realized by the time of doubling in the 0.25% integration. In the 4% integration, this fraction is about 40%. For all the transient integrations, the fraction of the equilibrium response realized by the time of CO_2 doubling is much less than 1.0 due to the large effective thermal inertia of the oceans. However, as will be shown later, the fraction of the equilibrium response for surface air temperature by the time of doubling is much larger than that for the steric sea level rise.

The magnitude of the response at the time of CO_2 doubling, as seen in the global mean surface temperature response described earlier, is much larger in the integrations with the slower rate of increase in the atmospheric CO_2 concentration. But in all these cases the transient response pattern (Fig. 6) differs significantly from the equilibrium response pattern (Fig. 3). The relative minimum in the warming found in the northern North Atlantic and Circumpolar Ocean region in the transient integrations is not seen in the equilibrium surface air temperature response. This points to the very long adjustment timescales found in these regions of the ocean. The degree to which the transient response patterns are similar to each other, and not to pattern found in the equilibrium 2X-integration, is impressive. This suggests that the rate of CO_2 increase would have to be much smaller than the slowest rate used here (0.25%) for the transient SAT response pattern to be similar to that obtained from the equilibrium 2X-integration.

As discussed earlier, the warming over the continents is generally larger than the warming over the oceans at the same latitude in the equilibrium 2X-integration. In the transient integrations this land-sea contrast in the warming is even larger than in the equilibrium 2X-integration as shown previously by Manabe et al. (1992) and as evident from the normalized warming patterns of Fig. 7. These patterns were computed by dividing the magnitude of the warming in each location by the corresponding global mean, so that the global mean value for each map is 1. Manabe et al. found that in addition

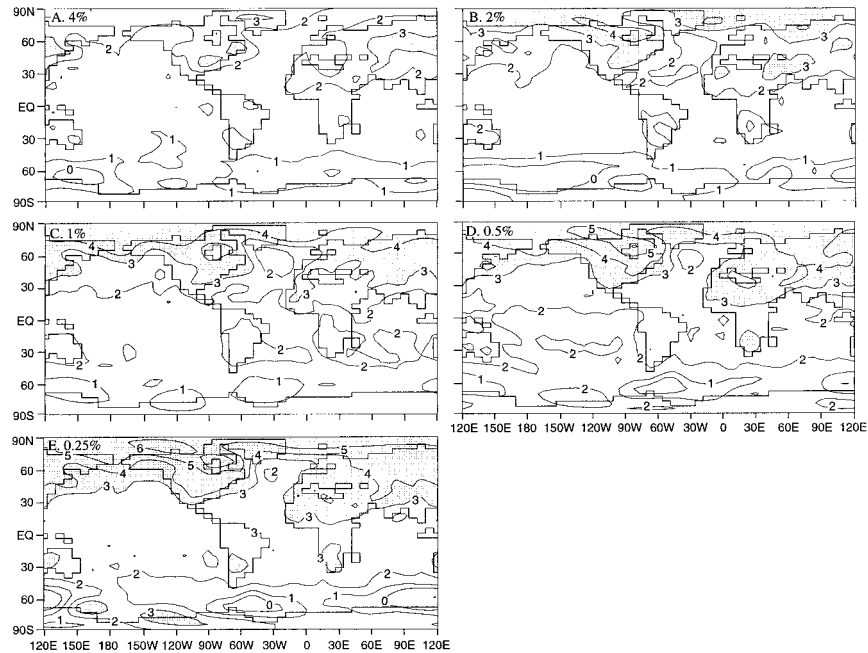


FIG. 6. Geographical distribution of the surface air temperature difference (K), transient minus the control integration around the time of CO_2 doubling: (a) 4% integration, (b) 2% integration, (c) 1% integration, (d) 0.5% integration, (e) 0.25% integration. The contour interval is 1 K. See Table 1 for the time periods used to compute the differences.

to the mechanisms that lead to the land–sea contrast in the warming in the equilibrium experiment discussed earlier, the thermal inertia of the oceans leads to an even larger land–sea contrast in the warming, which is enhanced by the increased summer drying of the land surface as described below.

Due to the larger thermal inertia of the oceans, the warming of the sea surface temperatures in middle and high latitudes of the Northern Hemisphere in the transient integrations is smaller than in the equilibrium 2X-integration. This leads to a reduction in the increase in evaporation over the oceans, which occurs in response to increased CO_2 in the atmosphere. Therefore, the CO_2 -induced increase in the moisture transport from the oceans to the continents is not as large as in the equilibrium experiment. This explains why the reduction of soil moisture over the continents is larger in the transient than the equilibrium 2X-integration. The drier continental surface then leads to a relatively larger warming in the transient integrations when compared to the equilibrium 2X-integration, because a relatively larger fraction of the heating due to the increase in CO_2 is available to warm the surface rather than enhance the evaporation. This leads to a larger land–sea contrast in the warming in the transient integrations (Fig. 7). Further analysis shows that the land–sea contrast in the warming is larger for the integrations with faster rates of CO_2 increase. The slower rates of CO_2 increase allow the ocean to be in closer equilibrium with the radiative forcing.

b. Thermohaline circulation

In response to increasing atmospheric CO_2 concentration, the THC weakens in all the transient integrations (Fig. 8). This reduction of the THC in response to increasing CO_2 was discussed earlier by M91 and is also found in other coupled model transient CO_2 simulations (Kattenberg et al. 1996). The integration (Fig. 8) with the slowest rate of increase of atmospheric CO_2 (0.25%) has the largest reduction in the maximum value of the THC in the northern Atlantic Ocean by the time of CO_2 doubling, while the integration with the fastest rate of increase in atmospheric CO_2 (4%) has only a very small reduction by the doubling time.

Figure 9 shows the streamfunction of the meridional circulation in the Atlantic Ocean of the 4% and 0.25% integrations at the time of CO_2 doubling. By comparing Fig. 9a to 9b, one notes that in the 4% integration the change from the control integration is very small, while in the 0.25%, the circulation is much weaker and shallower. The shallowing can be seen by looking at the placement of the 0 Sv ($\text{Sv} \equiv 10^6 \text{ m}^3 \text{ s}^{-1}$) contour. In the 4% integration, this contour intersects the bottom at about 30° N , while south of this latitude, the depth of this contour is about 2.5 km. In the 0.25% integration, the depth of the 0 Sv contour is shallower and intersects the bottom at about 60° N . By studying temperature and salinity characteristics of the waters in areas of negative streamfunction values near the bottom of the Atlantic Ocean, we have found that they are typically of Ant-

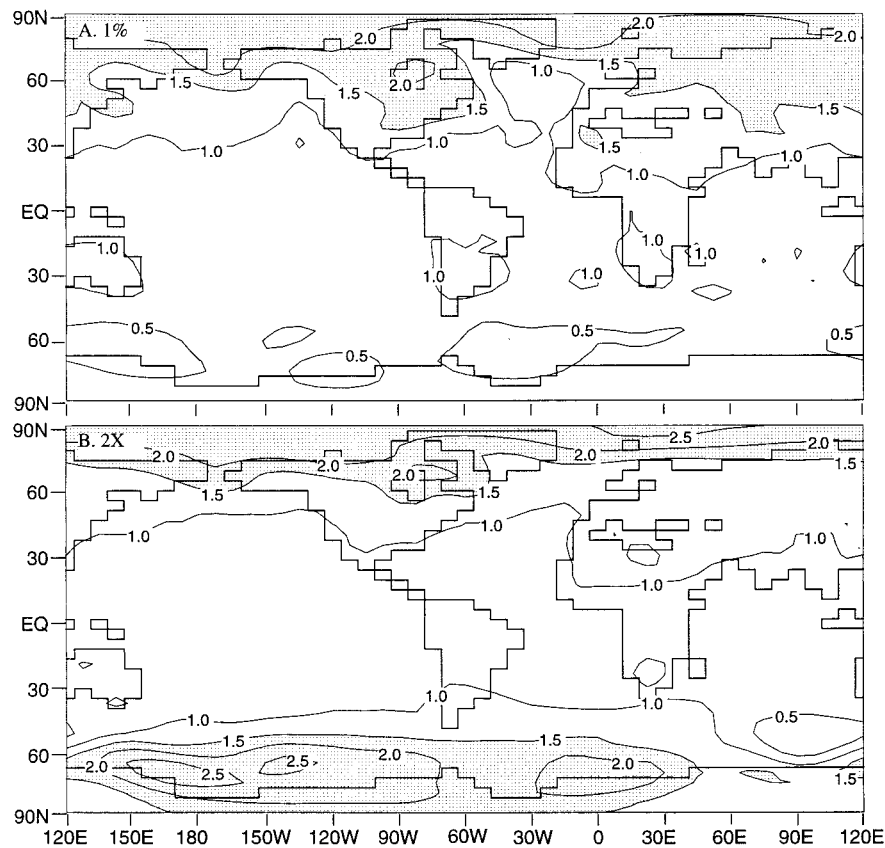


FIG. 7. Geographical distribution of the normalized surface air temperature response, or the surface air temperature response at each gridpoint divided by the global mean response for each figure: (a) 1% response at the time of CO₂ doubling, (b) equilibrium 2X response. See Table 1 for the periods used to compute the differences.

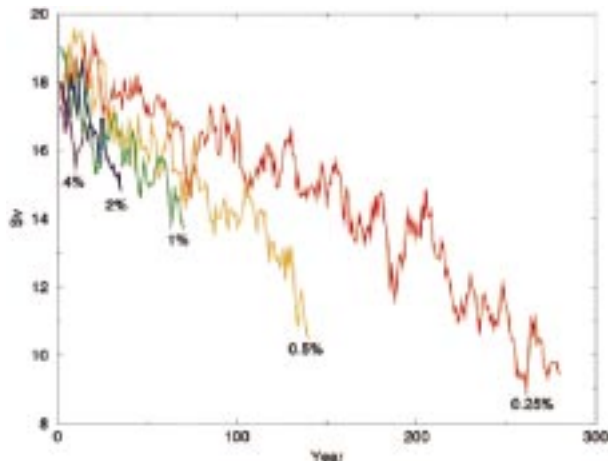


FIG. 8. Time (yr) series of the maximum value of the streamfunction ($Sv \equiv 10^6 \text{ m}^2 \text{ s}^{-1}$) between 40°N and 60°N in the Atlantic Ocean for the various integrations: 0.25% (red), 0.5% (orange), 1% (green), 2% (blue), and 4% (purple).

arctic origin. Thus, the shallowing of the 0 Sv contour in the 0.25% integration indicates that waters found at the bottom of the North Atlantic Ocean have become more Antarctic in origin.

The weakening and shallowing of the THC mainly results from the increasing supply of freshwater at the surface over the sinking regions of the THC as described by M91 and Dixon et al. (1999, manuscript submitted to *Geophys. Res. Lett.*). They showed that, associated with the global warming, the absolute humidity of the air increases, enhancing the poleward moisture transport in the troposphere. The enhanced moisture transport, in turn, causes a marked increase in precipitation in high latitudes, capping the oceanic surface with relatively fresh, low density water. This capping reduces the convective activity and negative buoyancy production in the sinking region of the THC, thereby reducing its intensity.

As the intensity of the THC decreases, the time that the surface waters in the high latitudes remain in contact with the atmosphere before sinking, lengthens. Since the high latitudes are regions where precipitation exceeds evaporation, the longer surface water residence

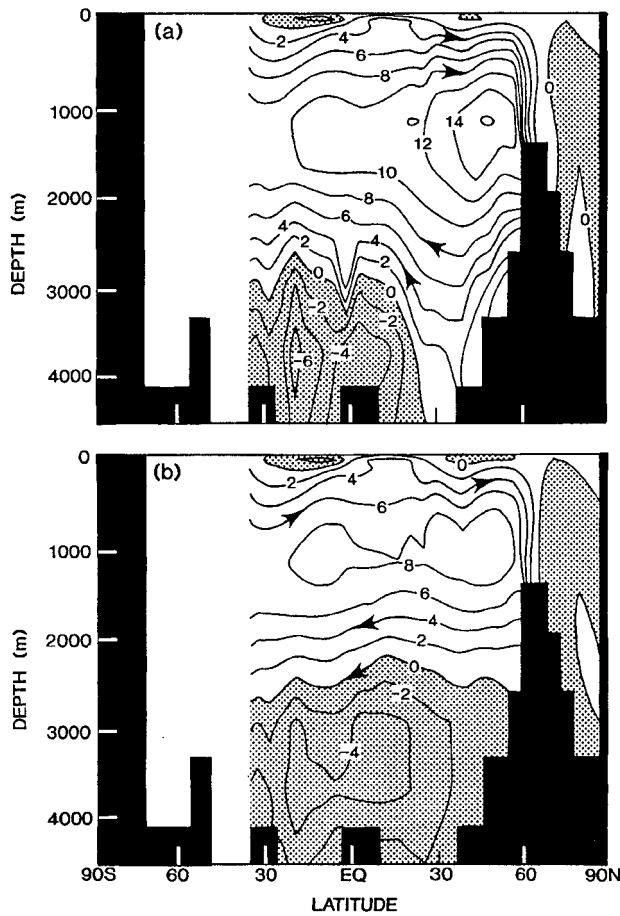


FIG. 9. Latitude–depth distribution of the meridional streamfunction in the Atlantic Ocean (Sv). (a) The 4% integration and (b) the 0.25% integration. The contour interval is 2 Sv. Negative values are shaded. See Table 1 for the periods used to compute the time averages.

times allow them to become even fresher before sinking, a positive feedback. These processes are opposed by density changes throughout the deeper levels of the ocean, which tend to restore the THC to its original intensity (M94). The weakening processes of the THC, which involve changes in the atmosphere and upper ocean have much faster timescales than the restoring timescales, which involve the deeper levels of the ocean. Thus as the time to CO_2 doubling lengthens, there is more time available for the capping of the oceanic surface before the density changes in the deeper layers of the ocean become large enough to reintensify the THC. This is why the total weakening of the THC due to the CO_2 doubling is largest in the integration using the slowest rate of CO_2 increase (0.25%) as indicated by Table 3.

An interesting question that arises in these integrations described here is: what happens to the THC after the CO_2 stops increasing? M94 found that the THC continued to decrease after the CO_2 concentration in the atmosphere stopped increasing in their 2XC integration. (The rate of CO_2 increase in this integration was 1%

TABLE 3. North Atlantic THC at doubling for the various integrations. Max THC is the maximum value of the thermohaline circulation in the North Atlantic Ocean in the various integrations. Diff is the total weakening by the time of CO_2 doubling of the Max THC. Units are in Sv. Cntrl Cpld is the value of the Max THC in the control integration of the coupled model, while Equil. Cpld is the maximum value in the equilibrium 2X-integration.

Exp. Name	0.25%	0.5%	1%	2%	4%	Equil. Cpld	Cntrl Cpld
Max THC (Sv)	10	12	13	15	18	18	18
Diff	8	6	5	3	0		

per year, so that the CO_2 doubled by year 70. After that point, the CO_2 concentration was held fixed at twice the normal value.) The weakening continued to about year 150, 80 yr after the CO_2 stopped increasing (Fig. 10). After year 150 in the 2XC integration, the THC slowly regained its original intensity.

To determine if the continued weakening of the THC after the CO_2 stopped increasing is dependent on the rate of CO_2 increase, the 0.25% integration is continued from year 280 to year 500 with the CO_2 concentration fixed at twice the normal value. In the 0.25% integration, CO_2 doubles at year 280. From Fig. 10, one notes that after a period of little change from about year 280 to year 380, the THC recovers. In this integration, the THC did not continue to weaken after the CO_2 concentration in the atmosphere stopped increasing as was the case for the 1% integration. This indicates that for slow rates of increase in the CO_2 concentration, the thermal structure of the ocean has more time to adjust by the time of CO_2 doubling.

By comparing the minimum THC value reached in the two integrations (Fig. 10), one observes that the total amount of weakening in the two integrations is very similar. From this result, it appears unlikely that the

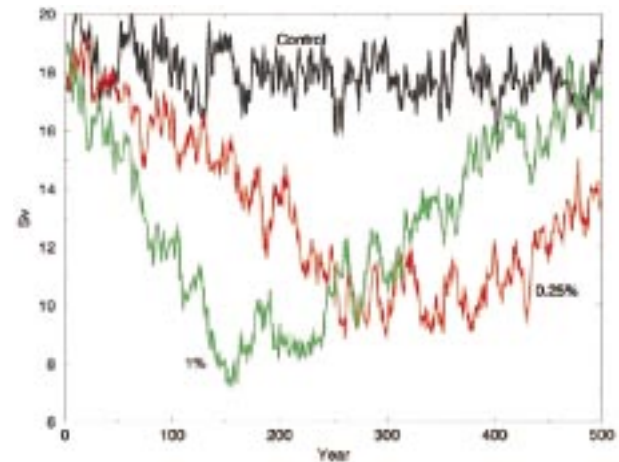


FIG. 10. Time (yr) series of the maximum value of the streamfunction (Sv) between 40° N and 60° N in the Atlantic Ocean for the control (black line), 1% (green line), and 0.25% (red line) integrations.

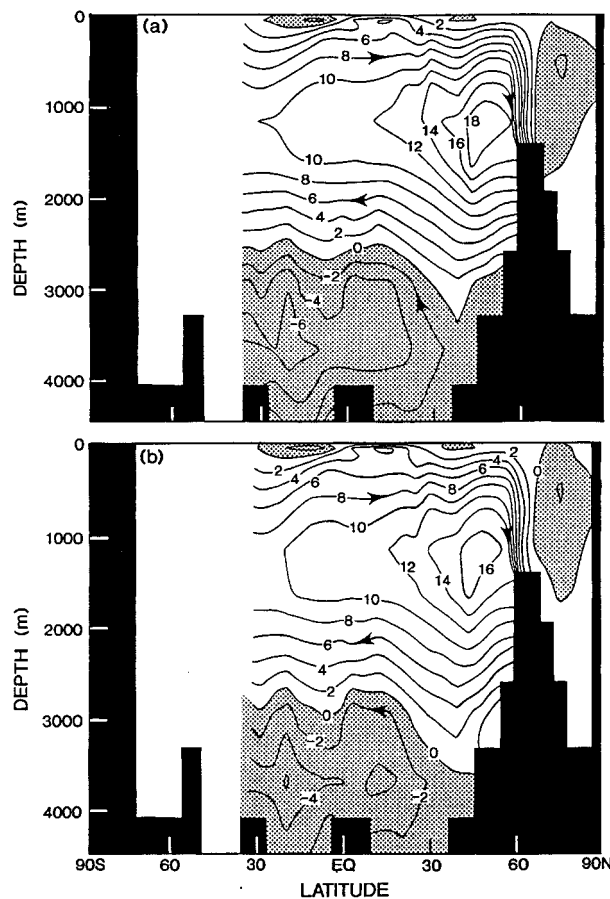


FIG. 11. Latitude depth distribution of the meridional streamfunction in the Atlantic Ocean (Sv) for years 3901–4000 of (a) the 2X-integration and (b) the control integration. The contour interval is 2 Sv. Negative values are shaded.

THC collapses in the North Atlantic Ocean for total changes of CO_2 smaller than doubling. In addition, these results suggest that the likelihood of a collapse of the THC after the atmospheric CO_2 stops increasing is smaller when the rate of CO_2 increase is smaller.

As indicated in Table 3, the intensity of the THC is similar between the two equilibria obtained from the control and 2X-integrations, while in all the transient CO_2 integrations the THC is weaker than the equilibrium values. After the THC reintensifies, its strength remains near the control value during the remainder of the 2X-integration. Not only is the maximum intensity of the THC in the Atlantic very similar between the 2X-integration and the control, but the pattern of the streamfunction contours is also surprisingly similar (Fig. 11). The flow in and out of the basin at 30°S is about 10 Sv in both experiments. The Antarctic bottom water flow at depth in the southern part of the basin is about 4 Sv in both experiments. And finally, the maximum value of the THC is very similar between the two experiments; just over 18 Sv in the 2X-integration and just under 18 Sv in the control.

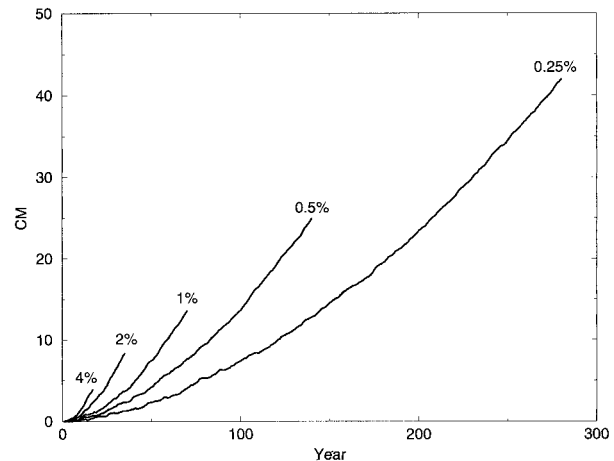


FIG. 12. Time (yr) series of global mean sea level rise (cm) due only to the changes in density for the various integrations. The trend in the control integration is removed by subtracting the exact corresponding time periods between the transient and control integrations.

The similarity of the THC between the two equilibrium integrations using normal and high CO_2 concentrations in the atmosphere was found previously by Manabe and Bryan (1985) in a model with idealized geography. As discussed in their paper, if the waters warmed uniformly everywhere in response to the increased atmospheric CO_2 , the nonlinear dependence of seawater density upon temperature would cause the density reduction of the low-latitude water to be larger than the high-latitude water. This would increase the meridional density gradient. On the other hand, the polar amplification of the surface warming and the decrease in surface salinity in high latitudes (as discussed earlier) contribute to the reduction of the meridional density gradient. Because of the compensation between these opposing effects, the meridional density gradient hardly changes between the normal and doubled CO_2 equilibrium states. The similarity of the meridional density gradient between the two equilibrium integrations accounts for the similarity in the intensity of the THC.

c. Sea level rise

The largest globally averaged steric sea level rise (due only to the thermal expansion of the seawater) by the time of CO_2 doubling occurs in the integration with the 0.25% integration (42 cm: Fig. 12, Table 4). Unlike the corresponding surface air temperature results, the ratio of the transient to equilibrium response in this integration is quite small, with a value less than 0.25. This fraction is even smaller for the other transient integrations. This implies that sea level continues to rise long after the CO_2 stops increasing in the model's atmosphere. The continued increase in sea level is due to the

TABLE 4. Sea level rise at doubling for the various integrations. Sea level rise is the sea level difference between the given integration and the control integration for the same time period. Here sea level rise is only due to the expansion of the water due to the density changes caused by temperature and salinity changes in response to the increasing CO_2 in the atmosphere. FRAC is the fraction of the total sea level rise response, computed by dividing the sea level rise from the given integration by the sea level rise of the equilibrium 2X-integration.

Exp. Name	0.25%	0.5%	1%	2%	4%	Equil. Cpld
Sea level rise (cm)	42	27	15	9	5	187
FRAC	0.22	0.14	0.08	0.05	0.03	1.0

slow downward penetration of the temperature anomaly in the ocean (M94).

This slow penetration results from the fact that surface waters mix with deep waters in only a few places in the high latitudes of the oceans (Fig. 13). Over most of the ocean surface, the heat anomaly due to increased CO_2 in the atmosphere penetrates only to depth via the slow process of diffusion. By the time of doubling in the 4% integration (Fig. 13a), the water warms only within a few hundred meters of the surface. In the 0.25% integration (Fig. 13b), the warming penetrates to depth in high latitudes. However, even in this integration where the CO_2 doubles at year 280, the warming is less than 0.5 K below 1.5 km in middle and low latitudes. The relatively small temperature change at depth in response to increasing CO_2 is responsible for the relatively small sea level rise (Fig. 12). In the integrations with slower rates of CO_2 increase, there is more time for the heat to penetrate to depth in the ocean, leading to relatively larger rises in sea level.

From Table 4, one notes that the steric rise of sea level becomes very large (1.9m) when the coupled model has time to equilibrate with twice the normal atmospheric CO_2 concentration. This value is much larger than that found in any of the transient integrations. As discussed earlier, the temperature increased by about 3.5 K throughout the whole ocean (Fig. 4), accounting for the large sea level rise. This relatively large rise in sea level results only from the thermal expansion of the ocean. In addition, any changes in land ice volume would add to or subtract from this large rise. Most of this rise in sea level occurs long after the atmospheric CO_2 amount was stabilized.

6. Conclusions

By the time of CO_2 doubling, the integration with the slowest rate of increase in atmospheric CO_2 concentration has the largest SAT increases, both locally and globally. The integration with slowest rate of increase of CO_2 , the 0.25% integration, had the largest globally averaged change in SAT (2.6 K). This is about 58% of the equilibrium response. The fastest rate of increase of atmospheric CO_2 , produced the smallest globally av-

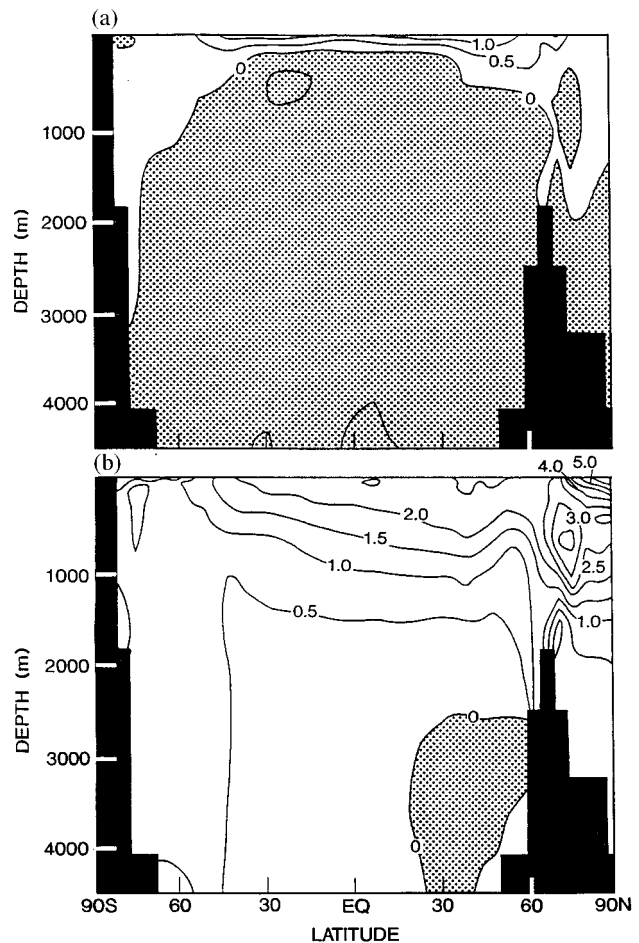


FIG. 13. Latitude–depth distribution of the zonal-mean temperature difference (K) at the time of CO_2 doubling, transient minus the control integration (a) the 4% integration and (b) the 0.25% integration. The contour interval is 0.5 K. Negative values are shaded. See Table 1 for the time periods used to compute the differences.

eraged SAT increase at the CO_2 doubling time (1.5 K), which is about 33% of the equilibrium value. Thus at the time of doubling, the slower the rate of increase in atmospheric CO_2 concentration, the closer the response of SAT is to the equilibrium value.

Confirming results from earlier studies, an SAT warming minimum in the northern North Atlantic and Circumpolar Oceans occurs in response to increasing CO_2 in the atmosphere for all the transient integrations shown here. This minimum in the warming in the transient integrations is due to the deep penetration of the temperature anomaly into the oceans in these regions. The degree to which the pattern of the SAT warming obtained from the transient integrations with increasing atmospheric CO_2 concentration are similar to each other, and not to the pattern obtained from the equilibrium 2X-integration, points to the long adjustment timescales found in the ocean.

In the equilibrium 2X-integration, there is a land–sea

contrast in SAT warming with larger warming over the continents compared to the adjacent oceans. First, the continental surface is drier than the oceanic surface and it dries further in response to the increase of CO_2 . Therefore, evaporation is less effective in moderating the surface warming over the continents than over the oceans. Second, the coverage of snow over the continents is much more extensive than that of sea ice over the oceans. Thus, the albedo feedback process is more effective in enhancing the surface warming over the continents than over the oceans poleward of 40°N . In the transient experiments, the difference in the heat capacity of the underlining surface makes the land–sea contrast in the warming even larger. The relatively small heat capacity of the continental surface allows the SAT response to increasing CO_2 to be larger over the land than over the ocean. Further, we found that the faster the rate of increase in atmospheric CO_2 concentration in the transient integrations, the larger the land–sea contrast in the SAT warming.

The fraction of the equilibrium steric sea level rise that occurs by the time of CO_2 doubling is much smaller than the corresponding fraction for globally averaged SAT response. Heat anomalies can penetrate to depth on short timescales only in a few places in the World Ocean. Over the rest of the World Ocean, heat only slowly reaches the ocean interior. This slow penetration of heat into the World Ocean leads to relatively small steric sea level rises by the time of CO_2 doubling in the transient integrations. In integrations where the rate of CO_2 increase is slower and therefore takes longer to reach CO_2 doubling, the steric rise of sea level is larger because there is more time for the heat anomaly to penetrate to depth in the ocean. The fact that only a relatively small fraction of the equilibrium steric rise of sea level is realized by the time of CO_2 doubling in the transient experiments implies that there is a relatively large sea level rise after the CO_2 concentrations are stabilized.

Studies using simpler models have described how the response of the global mean surface temperature and global mean sea level depend upon the rate of increase in the greenhouse gas concentrations. Many of these studies use an upwelling–diffusion model similar to that developed by Hoffert et al. (1980). This type of model couples an energy–balance atmosphere model with an upwelling–diffusion model of the oceans and is used to study the response of global mean surface temperature and sea level to changes in the radiative forcing of the coupled system. Because the model can be integrated very efficiently, experiments using many different forcing scenarios can be run and the results analyzed. However, since the strength of the vertical mixing is set as a constant for the duration of the integration, any time-dependent changes in the ocean circulation, horizontal or vertical, are not simulated by this model. Many different studies have used this type of model to study the response of the coupled atmosphere–ocean system to

changes in forcing (e.g., Hoffert and Flannery 1985; Wigley and Raper 1987; Wigley 1989; Wigley 1991; Schlesinger and Jiang 1991). The paper by Wigley and Raper (1992) is a good example of a study that uses a model of this type to investigate the impact of various greenhouse gas scenarios on global mean temperature and sea level rise for use in the IPCC 1992 report.

In the IPCC 1995 report, Kattenberg et al. (1996) conduct a comparison of the latest upwelling diffusion model of Wigley with the present SAT results using the fully coupled ocean–atmosphere model. The comparison (see Fig. 6.13 in the IPCC 1995 report) shows that the upwelling diffusion model can be tuned to accurately simulate the time-dependent behavior of the global mean SAT obtained from the fully coupled model over a wide range of rates of increase in the CO_2 concentration. They also compare the upwelling diffusion model results with the 2XC and 4XC fully coupled integrations of M94. Again, the results from the simple model are similar to those obtained from the coupled model used here for the doubled CO_2 concentration integration (2XC) for both global mean surface air temperature and for steric sea level rise. However, the comparison shows that by the end of the four times the normal CO_2 concentration (4XC) integration, the upwelling diffusion model has a smaller warming and a smaller steric sea level rise than does the fully coupled model. Kattenberg et al. thus conclude that this model, if properly tuned, can successfully emulate the coupled model results shown here for changes in global mean surface air temperature and steric sea level rise as long as there are no large changes in ocean circulation such as is found in the results from the 4XC integration.

In the coupled model used here, the THC weakened in all the transient integrations in response to the increasing CO_2 concentration in the atmosphere, confirming earlier studies. M91 discussed how the weakening and shallowing of the THC mainly occurs in response to the increasing supply of freshwater at the surface over the sinking regions of the THC. The CO_2 -induced increase in absolute humidity associated with global warming in the troposphere increases the poleward moisture transport in the atmosphere. The enhanced poleward transport causes a marked increase in the precipitation and runoff in high latitudes, increasing the supply of freshwater at the ocean surface. This caps the ocean surface with relatively fresh, low density water, which in turn reduces the convective activity and negative buoyancy production in the sinking region of the THC, thereby slowing down the overturning.

If it takes longer for the CO_2 to double, more time is available for the capping to become effective. Therefore the transient integrations with the slower rates of CO_2 increase have a larger weakening of the THC by the time of CO_2 doubling. For example, the THC in the 0.25% integration weakens from a value of about 18 Sv in the control integration to 10 Sv by the time of doubling. In the integration with the fastest rate of increase, the 4%

integration, the THC hardly weakens in the 17 yr it takes CO₂ to double in this integration. These results suggest that the rate of CO₂ increase has a significant impact on the magnitude of the changes in the thermal and dynamical structure of the coupled ocean–atmosphere system realized by the time of CO₂ doubling.

In the earlier study of M94, it was found that after an initial period of weakening the THC in their 2XC integration (the 1% integration here) eventually recovered to its original intensity after the atmospheric CO₂ stopped increasing. Furthermore, it is found here that the intensity of the THC remains at this original level through the end of the 4000-yr integration when a stable equilibrium state was reached. The similarity of the THC in the control and 2X-integrations results from the compensation of opposing effects on the meridional density gradient. The decrease in surface salinity in high latitudes as discussed above and the polar amplification of the surface air temperature response tend to decrease the meridional density gradient. On the other hand, because of the nonlinear dependence of temperature on the density of seawater, the meridional density gradient tends to increase, in association with the warming. These effects tend to counter balance each other so that the meridional density gradient and therefore the THC, hardly change between the equilibrium states.

In the 2XC integration of M94, it was noted that although the CO₂ stopped increasing at year 70 of the integration, the THC continued to weaken to year 150 before recovering. To investigate the effect of the rate of CO₂ increase on this overshoot of the THC, the 0.25% integration is also continued beyond the doubling time, holding the CO₂ concentration fixed at twice the normal amount. We found that the amount of weakening of the THC after the CO₂ stopped increasing is reduced for the 0.25% integration because the ocean has more time to adjust by the time of CO₂ doubling. This is in contrast to the results from the 1% integration described above where the THC continued to weaken after the CO₂ stopped increasing. In both the 1% and 0.25% integrations, the THC eventually recovers to the control integration value.

Manabe and Stouffer (1988) found that the modeled THC in the Atlantic has two stable states, one where the THC is active (as in today's climate) and the other in which the THC is inactive in the North Atlantic Ocean. Further, the results of M94 showed that the THC can switch from the active stable state to the inactive state in this model when the rate of CO₂ increase is 1% yr⁻¹ and sustained for 140 yr until the atmospheric CO₂ quadruples. The overshooting behavior of the THC described above could possibly lead to the case where the THC changes states from active to inactive even after the CO₂ concentration in the atmosphere stops increasing. Once the THC shuts down and deep water formation stops in the North Atlantic Ocean, there is the possibility that the THC may never restart or remain inactive for a very long time period.

Recently Stocker and Schmittner (1997) using an energy balance atmosphere model coupled to a two-dimensional ocean model, found that the rate of CO₂ increase affects the amount of THC weakening at a given CO₂ concentration. These results are confirmed here using a three-dimensional coupled ocean–atmosphere general circulation model. In addition, they found that the THC goes into an inactive state when CO₂ increases at a rate of 1% yr⁻¹ for 100 yr. This result is consistent with those obtained by M94.

Finally, it is important to note features or processes where the transient response is unlike the equilibrium response. This is especially the case for the thermohaline circulation where, in response to increasing CO₂ concentration in the atmosphere, the THC weakens and shallows. However, the THC in the control and equilibrium 2X-integrations have similar intensities and streamfunction patterns. Given that some features of the transient response of climate to external forcings are sometimes very different from the equilibrium response, this makes the study of climate change both much more interesting and more difficult. The direction of the initial climate response to a given forcing is not necessarily the direction of the equilibrium response. This is found for all the transient integrations presented here, even for those where CO₂ doubling occurred more than one century after the integration began.

Acknowledgments. The authors wish to thank Tony Broccoli, whose ideas helped in the experimental design of these integrations. Tony Broccoli, Isaac Held, Jerry Mahlman, and Mike Winton gave us many helpful suggestions to improve the manuscript.

REFERENCES

- Bryan, K., 1984: Accelerating the convergence to equilibrium of ocean climate models. *J. Phys. Oceanogr.*, **14**, 666–673.
- , and L. J. Lewis, 1979: A water mass model of the world ocean. *J. Geophys. Res.*, **84**, 2503–2517.
- Cubasch, U., K. Hasselmann, K. Hock, E. Maier-Reimer, U. Mikolajewicz, B. D. Santer, and R. Sausen, 1992: Time-dependent greenhouse warming computations with a coupled ocean–atmosphere model. *Climate Dyn.*, **8**, 55–69.
- Delworth, T., S. Manabe, and R. J. Stouffer, 1993: Interdecadal variation of the thermohaline circulation in a coupled ocean–atmosphere model. *J. Climate*, **6**, 1993–2011.
- , —, and —, 1997: Multidecadal climate variability in the Greenland Sea and surrounding regions: A coupled model simulation. *Geophys. Res. Lett.*, **24**, 257–260.
- Dixon, K. W., J. L. Bullister, R. H. Gammon, and R. J. Stouffer, 1996: Examining a coupled air–sea model using CFCs as oceanic tracers. *Geophys. Res. Lett.*, **23**, 1957–1960.
- Fanning, A. F., and A. J. Weaver, 1997: A horizontal resolution and parameter study of heat transport in an idealized coupled climate model. *J. Climate*, **10**, 2469–2478.
- Gates, W. L., J. F. B. Mitchell, G. J. Boer, U. Cubasch, and V. P. Meleshko, 1992: Climate modelling, climate prediction and model validation. *Climate Change 1992: The Supplementary Report to the IPCC Scientific Assessment*, J. T. Houghton, B. A. Callander, and S. K. Varney, Eds., Cambridge University Press, 97–134.

- Gordon, C. T., and W. Stern, 1982: A description of the GFDL Global Spectral Model. *Mon. Wea. Rev.*, **110**, 625–644.
- Gregory, J. M., and J. F. B. Mitchell, 1997: The climate response to CO₂ of the Hadley Centre coupled AOGCM with and without flux adjustments. *Geophys. Res. Lett.*, **24**, 1943–1946.
- Haywood, J. M., R. J. Stouffer, R. T. Wetherald, S. Manabe, and V. Ramaswamy, 1997: Transient response of a coupled model to estimated changes in greenhouse gas and sulfate concentrations. *Geophys. Res. Lett.*, **24**, 1335–1338.
- Hoffert, M. I., and X. Flannery 1985: Model projections of the time-dependent response to increasing carbon dioxide. DOE/ER-0237, Office of Energy Research, Office of Basic Energy Sciences, Washington, DC, 381pp. [Available from National Technical Information Service, Technology Administration, U.S. Dept. of Commerce, Springfield, VA, 22161.]
- , A. J. Callegari, and C.-T. Hsieh, 1980: The role of deep sea storage in the secular response to climate forcing. *J. Geophys. Res.*, **85**, 6667–6679.
- Kattenberg, A., and Coauthors, 1996: Climate models—Projections of future climate. *Climate Change 1995: The Science of Climate Change*, J. T. Houghton et al., Eds., Cambridge University Press 285–357.
- Knutson, T. R., S. Manabe, and D. Gu, 1997: Simulated ENSO in a global coupled ocean–atmosphere model: Multidecadal amplitude modulation and CO₂ sensitivity. *J. Climate*, **10**, 138–161.
- Manabe, S., 1969: Climate and the ocean circulation. Part I: The atmospheric circulation and the hydrology of the earth's surface. *Mon. Wea. Rev.*, **97**, 739–774.
- , and K. Bryan, 1985: CO₂-induced change in a coupled ocean–atmosphere model and its paleoclimatic implications. *J. Geophys. Res.*, **90**, 11 689–11 707.
- , and R. J. Stouffer, 1988: Two stable equilibria of a coupled ocean–atmosphere model. *J. Climate*, **1**, 841–866.
- , and —, 1994: Multiple-century responses of a coupled ocean–atmosphere model to an increase of atmospheric carbon dioxide. *J. Climate*, **7**, 5–23.
- , and —, 1995: Simulation of abrupt climate change induced by freshwater input to the North Atlantic Ocean. *Nature*, **378**, 165–167.
- , and —, 1996: Low frequency variability of surface air temperature in a 1000-year integration of a coupled ocean–atmosphere model. *J. Climate*, **9**, 376–393.
- , and —, 1997: Coupled ocean–atmosphere model response to freshwater input: Comparison to Younger Dryas event. *Paleoceanography*, **12**, 321–336.
- , R. Wetherald, and R. J. Stouffer, 1981: Summer dryness due to an increase of atmospheric carbon dioxide concentration. *Climate Change*, **3**, 347–386.
- , R. J. Stouffer, M. J. Spelman, and K. Bryan, 1991: Transient responses of a coupled ocean–atmosphere model to gradual changes of atmospheric CO₂. Part I: Annual mean response. *J. Climate*, **4**, 785–818.
- , M. J. Spelman, and R. J. Stouffer, 1992: Transient response of a coupled ocean–atmosphere model to gradual changes of atmospheric CO₂. Part II: Seasonal response. *J. Climate*, **5**, 105–126.
- Marotzke, J., and P. Stone, 1995: Atmospheric transports, the thermohaline circulation and flux adjustments in a simple climate model. *J. Phys. Oceanogr.*, **25**, 1350–1364.
- Meehl, G. A., W. M. Washington, D. J. Erickson III, B. P. Briegleb, and P. J. Jaumann, 1996: Climate change from increased CO₂ and direct and indirect effects of sulphate aerosols. *Geophys. Res. Lett.*, **23**, 3755–3758.
- Mitchell, J. F. B., S. Manabe, V. Meleshko, and T. Tokioka, 1990: Equilibrium climate change—and its implications for the future. *Climate Change: The IPCC Scientific Assessment*, J. T. Houghton, G. J. Jenkins, and J. J. Ephraums, Eds., Cambridge University Press, 131–172.
- , T. C. Johns, J. M. Gregory, and S. F. B. Tett, 1995: Climate response to increasing levels of greenhouse gases and sulphate aerosols. *Nature*, **376**, 501–504.
- Murphy, J. M., and J. F. B. Mitchell, 1995: Transient response of the Hadley Centre coupled ocean–atmosphere model to increasing carbon dioxide. Part II: Spatial and temporal structure of the response. *J. Climate*, **8**, 57–80.
- Schlesinger, M. E., and X. Jiang, 1991: Revised projection of future greenhouse warming. *Nature*, **350**, 219–221.
- Spelman, M. J., and S. Manabe, 1984: Influence of oceanic heat transport upon the sensitivity of a model climate. *J. Geophys. Res.*, **89** (C1), 571–586.
- Stocker, T. F., and A. Schmittner, 1997: Influence of CO₂ emission rates on the stability of the thermohaline circulation. *Nature*, **388**, 862–865.
- Stouffer, R. J., S. Manabe, and K. Bryan, 1989: Interhemispheric asymmetry in climate response to a gradual increase of atmospheric CO₂. *Nature*, **342**, 660–662.
- , —, and K. Ya. Vinnikov, 1994: Model assessment of the role of natural variability in recent global warming. *Nature*, **367**, 634–636.
- Washington, W. M., and G. A. Meehl, 1989: Climate sensitivity due to increased CO₂: Experiments with a coupled atmosphere and ocean general circulation model. *Climate Dyn.*, **4**, 1–38.
- Wigley, T. M. L., 1989: Possible climate change due to SO₂-derived cloud condensation Nuclei. *Nature*, **339**, 365–367.
- , 1991: Could reducing fossil-fuel emissions cause global warming? *Nature*, **349**, 503–506.
- , and S. C. B. Raper, 1987: Thermal expansion of sea water associated with global warming. *Nature*, **330**, 127–131.
- , and —, 1992: Implications for climate and sea level of revised IPCC emission scenarios. *Nature*, **357**, 293–300.